An Investigation into the Corrosion Rates of Inconel 600™ in Different Corrosive Solutions

Brandon Davoren[a], Ernst E. Ferg[a,b,*] [§] and Nico Rust[b]

[a]*Department of Chemistry, Nelson Mandela University, P.O. Box 77000, Port Elizabeth, 6031, South Africa.*
[b]*uYilo, e-Mobility Technology Innovation Programme, Nelson Mandela University, P.O. Box 77000, Port Elizabeth, 6031, South Africa.*

Received 11 October 2018, revised 24 June 2019, accepted 24 June 2019.

ABSTRACT

Inconel 600™, an austenitic high nickel alloy, has relatively low corrosion properties and is used extensively for aerospace and nuclear engineering applications. Other applications include exposure of the material to caustic and acidic environments and possible use in prosthetic implants. Electrochemical techniques, which include potentiodynamic polarization and polarization resistance, provide a means to rapidly determine the corrosion rates and the suitability of the alloy in a specific corrosive environment. The results from these two techniques were used to determine the corrosion rates as well as other thermodynamic properties for the alloy exposed to various strong and weak acids, salt and Ringer's solution. The results showed slight differences in the corrosion rates determined by the two electrochemical techniques, with those from the polarization resistance technique being on average larger. The corrosion activation energies determined for the alloy in different solutions were indicative of the corrosion rates with some anomalies in values for results observed in the 10 % acetic acid solution. The microstructural composition of the alloy was also investigated by SEM-EDS and showed peculiar inclusions that can contribute to an acceleration of the corrosion rates.

KEYWORDS

Inconel 600, corrosion rates, potentiodynamic polarization, polarization resistance, activation energy.

1. Introduction

Inconel 600™ is a trademark of Inco Alloys International and is also referred to as Alloy 600.[1] It was originally developed for milk cans in the 1940s and is now used in a variety of industries including high temperature and pressure water reactors in the nuclear industry.[2,3] Its high nickel and chromium percentage makes it a specialized super alloy which is used when normal stainless steels would not suffice in high temperature applications. The typical elemental composition range of the alloy is summarized in Table 1 and the analytical set of results as determined by X-ray fluorescence (XRF) spectroscopy for the alloy samples used in this study are also shown.[1]

Inconel 600™ is utilized in many different highly corrosive and high temperature environments with some of the most noteworthy being the chemical manufacturing industry, aerospace, nuclear engineering components and gas turbine components.[2] In other studies, the corrosion behaviour of Inconel 600™ and Inconel 601™ were examined in solutions of orthophosphoric acid, between concentrations of 0.5 N and 15 N.[4] Inconel 600™ was found to have a smaller passivation range than Inconel 601™ and was also found to be more corrosive. The studies showed that the corrosion rates at ambient temperature would typically vary between 0.040 to 1.097 mm yr^{-1} in acid solutions of 0.5 N to 15 N, respectively.[4] In another study, the anodic corrosion behaviour of Inconel 600™ in sulphuric acid was studied by means of anodic polarization and electrochemical impedance spectroscopy (EIS).[5] The corrosion rates reported varied between 0.033 and 0.8344 mm yr^{-1} and were obtained in solutions that varied between 0.01 M to 10.00 M, respectively. Extensive studies in using Inconel 600™ in nitric acid and caustic soda applications were performed by Abdallah *et al.*[6–8] They made use of cyclic voltammetry to investigate the formation of the passivation film and compared it to other alloys such as Incoloy 800 and 316 stainless steel.

Table 1 The actual and recommended elemental composition range of Inconel 600™ alloy used in this study.

Element	XRF analysis content* /% by mass	Recommended** /% by mass
Ni	72.34	72.0 minimum
Cr	16.15	14.0–17.0
Fe	9.47	6.0–10.0
C	Below LoD (0.0)	0.15 maximum
Mn	0.64	1.00 maximum
S	Below LoD (0.0)	0.015 maximum
Si	0.35	0.50 maximum
Cu	Below LoD (0.0)	0.50 maximum

*Composition of the alloy used in this study as determined by XRF.
**Recommended alloy composition range.[1]

Balamurugan *et al.*[9] reviewed the use of specialty alloys in biomedical devices that can range from prosthetic limbs to dental implants and pacemakers. All metallic-based inserts are susceptible to corrosion and are usually studied by exposing them to a Ringer's solution that simulates the properties of bodily fluids.[9]

In this study, the corrosion properties Inconel 600™ were analyzed by using two slightly different electrochemical techniques when the alloy was exposed to a range of different acids and other typical corrosive solutions at various temperatures. The respective corrosion rates and thermodynamic activation energies of corrosion were determined and compared.

* To whom correspondence should be addressed.
E-mail: ernst.ferg@mandela.ac.za

ISSN 0379-4350 Online / ©2019 South African Chemical Institute / http://saci.co.za/journal
DOI: https://doi.org/10.17159/0379-4350/2019/v72a18

2. Experimental

Potentiodynamic polarization and linear polarization analyses were performed on a Princeton PAR 263A potentiostat. Cylindrical samples of the alloy were cast in resin allowing for only an area of 0.10 cm^2 to be exposed in the relevant solution. Samples were polished to a mirror finish by using a 3 μm diamond suspension. Once polished, the samples were allowed to stand in the relevant solution until a stable open circuit potential (OCV) was achieved. This would usually be achieved within one hour of equilibration time. All potentiodynamic polarization and linear polarization resistance experiments were performed in solutions that were prepared with de-aerated and deionized water.

The solutions used in this study were:

Ringer's solution: This was prepared by adding 9.0 g L^{-1} NaCl; 0.42 g L^{-1} KCl; 0.2 g L^{-1} $NaHCO_3$and 0.25 g L^{-1} $CaCl_2$ to distilled water and is the standard solution used to typically simulate human body fluid conditions in order to evaluate the corrosion characteristics of metal prosthetic inserts.[11]

3.5 % NaCl was prepared by adding AR grade NaCl to deionized water. This would typically simulate the concentration of sea water.

A solution of 25.8 % H_2SO_4 was prepared by adding AR-grade concentrated acid to distilled water. This was done typically to simulate the H_2SO_4 acid concentration used in lead acid batteries.

A range of HCl solutions were chosen at 0.74, 2.20, 3.70 and 7.40 % by mass by adding the correct amount by mass of AR-grade concentrated HCl to distilled water.

The range of acetic acid (HOAC) solutions were chosen to be 0.10, 1.00, 3.00, 5.00 and 10.00 % by mass by adding the correct amount of AR-grade concentrated acetic acid to distilled water.

A double-walled glass corrosion cell was used to conduct tests once stable temperatures were obtained within 1.0 °C. The temperatures chosen were 20, 25, 35, 45 and 50 °C.

Potentiodynamic polarization analysis was performed over a range of 100 mV in the anodic and cathodic regions either side of the E_{OC}. The step rate used was 2 mV s^{-1} and data points were recorded every 0.5 s. The same parameters were used at each successive temperature after waiting for the open circuit to stabilize.

The use of potentiodynamic polarization and polarization resistance allows for the rapid quantification of the corrosion rate (*CR*) of the alloy and the feasibility of its use in a specific environment. Potentiodynamic polarization analysis is performed by means of the Butler-Volmer equation and polarization resistance by the Stern-Geary equation.[10] By performing these electrochemical analyses at different temperatures (*T*) and by means of the Arrhenius equation, the activation energy (E_a) of the corrosion reaction can be described by using the linearized form of the Arrhenius Eq. 1.

$$\ln(CR) = \left(\frac{-E_a}{R}\right)\left(\frac{1}{T}\right) + \ln(A) \quad (1)$$

where *R* is the gas constant and *A* is the pre-exponential factor.

The transition state Eq. 2 was used to calculate the change in corrosion enthalpy (ΔH) and entropy (ΔS).

$$\ln\left(\frac{CR}{T}\right) = \ln\left(\frac{R}{Nh}\right) + \frac{\Delta S}{R} - \frac{\Delta H}{R}\left(\frac{1}{T}\right) \quad (2)$$

where *N* is Avogadro's constant and *h* is the Planck constant.

Polarization resistance was performed over a range of 25 mV in the anodic and cathodic regions either side of the E_{OC}. The step rate used was 2 mV s^{-1} and data points were recorded every 0.5 s. Polarization readings were performed directly after the relevant potentiodynamic polarization at a given temperature. The open circuit potential was allowed to stabilize and the electrode was only moved to remove any bubbles that may have formed on the surface of the alloy. Polarization resistance calculations were performed by using the respective anodic and cathodic Tafel coefficients obtained from the previous potentiodynamic polarization analysis. The corrosion currents obtained from both the potentiodynamic polarization and polarization resistance analysis were used to calculate the corrosion rates by means of the addition of the corrosion rates of each alloyed element by using Eqs. 3 and 4, respectively.

$$CR_{Element} = \%Element \times \left(\frac{I_{corr} \times M}{nF}\right) \quad (3)$$

$$CR_{Alloy}(g\ cm^{-2}\ s^{-1}) = \left(\frac{CR_{Element\,1}}{\rho_1}\right) + \left(\frac{CR_{Element\,2}}{\rho_2}\right) + \left(\frac{CR_{Element\,3}}{\rho_3}\right) + \cdots \quad (4)$$

where I_{corr} is the corrosion current density (μA cm^{-2}), *n* is the charge number, *M* is the molar mass of the element (g mol^{-1}) and ρ is the mass density (g cm^{-3}).

All electrochemical techniques were performed in duplicate.

For microstructural analysis, samples were polished to a mirror finish by using a 3.0 μm diamond suspension. The samples were then electrochemically etched with a solution of 10 g of chromic acid in 90 mL of deionized water. The grain size distribution was calculated by means of a Zeiss light microscope according to the ASTM E112-13 method.[12]

XRF analysis was semi-quantitative and was done on a Bruker S1 Titan handheld XRF in 'Alloys' mode.

3. Results and Discussion

As a representative example, the corrosion rates and relevant electrochemical data for Inconel 600™ alloy in Ringer's solution for both the potentiodynamic polarization and polarization resistance analysis at different temperatures are shown in Tables 2 and 3, respectively.

A graphical representation of the potentiodynamic polarization and the polarization resistance plots obtained at five successive temperatures in Ringer's solution are shown in Figs. 1 and 2, respectively.

The results showed that the corresponding corrosion rates (mm yr^{-1}) that were determined by potentiodynamic polarization plot analysis were slightly lower than those that were determined by polarization resistance measurements. The slight difference could be attributed to the fact that the polarization resistance measurements were performed over a much smaller potential range, which was the linear region of about 25 mV on either side of the OCV. The potentiodynamic polarization plot analysis would make use of about 100mV on either side of the OCV allowing for a larger set of data to be used in determining the corrosion current which would in turn also affect the corrosion rate. The results from the potentiodynamic polarization plot analysis can also be influenced by any additional pitting corrosion that could occur on the surface of the sample during analysis within the voltage range studied. Notably, the differences in the CR between the two techniques would also increase as the analysis temperature increased.

The calculated parameters and the Arrhenius equation (Eq. 1) were used to determine the activation energy as well as the change in corrosion enthalpy and entropy from the transition

Table 2 Potentiodynamic polarization parameters and corrosion rates (CR) of Inconel 600™ in Ringer's solution at different temperatures. E_{corr} = Corrosion potential; I_{corr} = corrosion current.

T /K	CR /10^{-5} mm yr^{-1}	E_{corr} /mV	I_{corr} /μA cm^{-2}	β_{cat} /mV	β_{an} /mV
293	7.52	–184.7	0.007388	97.417	176.332
298	10.0	–191.5	0.009837	94.412	127.927
308	22.6	–225.1	0.02217	102.500	121.373
318	57.6	–243.1	0.05663	115.008	112.025
323	80.1	–249.0	0.07875	124.362	123.693

Table 3 Polarization parameters of Inconel 600™ in Ringer's solution at different temperatures. CR = Corrosion rate; E_{corr} = corrosion potential; I_{corr} = corrosion current.

T /K	CR /10^{-5} mm yr^{-1}	R_p /Ω	E_{corr} /mV	I_{corr} /μA cm^{-2}
293	12.9	21.585	–210.7	0.01264
298	17.2	15.929	–209.0	0.01693
308	45.2	5.444	–264.5	0.04438
318	81.5	3.081	–266.0	0.08009
323	109.0	2.514	–270.8	0.10730

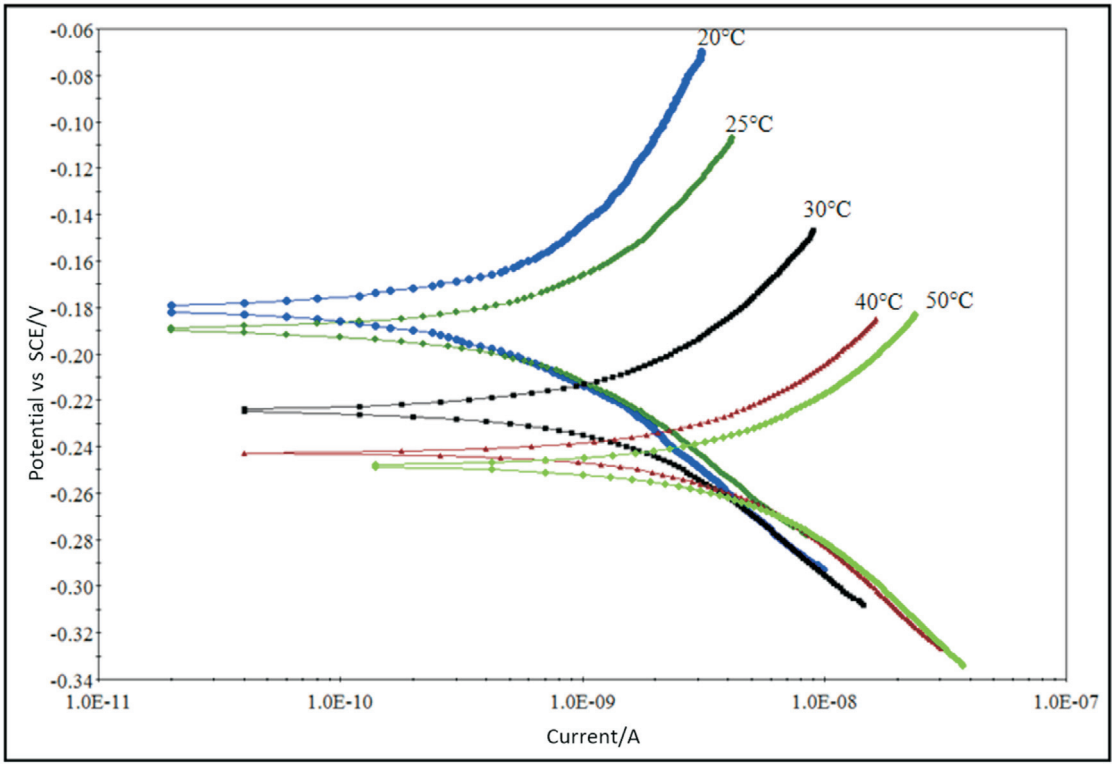

Figure 1 Potentiodynamic polarization plots at five successive temperatures in Ringer's solution.

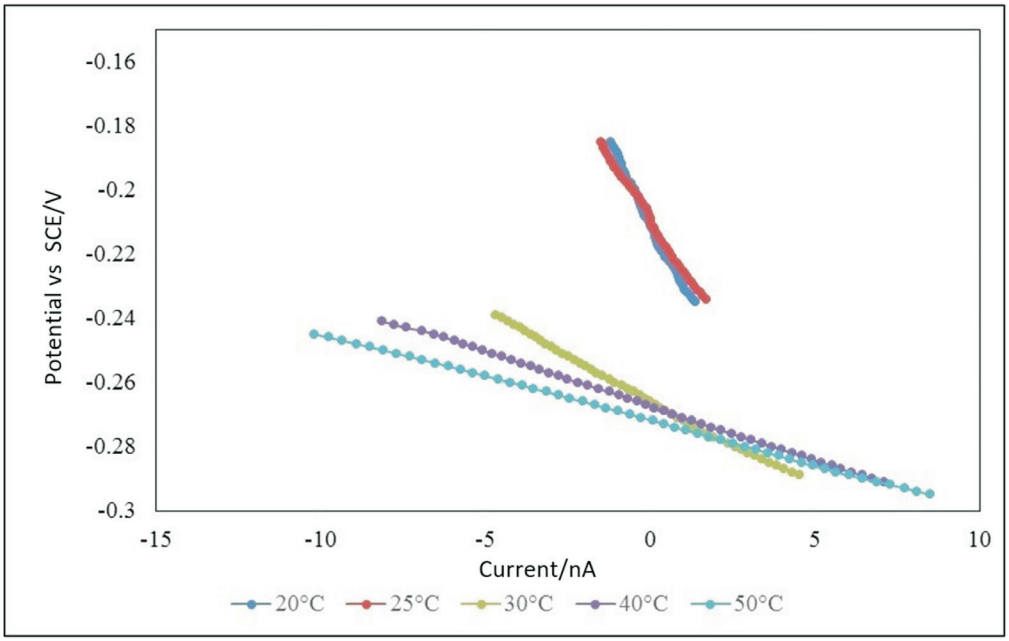

Figure 2 Linear polarization resistance plots at five successive temperatures in Ringer's solution.

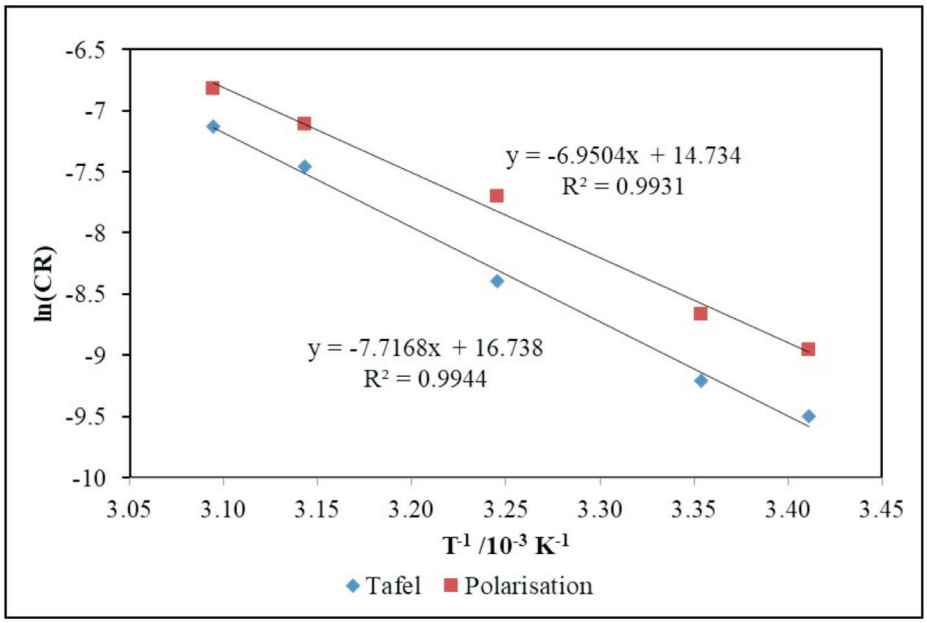

Figure 3 Linearlized Arrhenius plots of both potentiodynamic polarization and polarization resistance analysis of Inconel 600™ in Ringer's solution.

state (Eq. 2). As an example, the plots of the linearized form of the Arrhenius equation for both the potentiodynamic polarization and polarization resistance results of the analysis in Ringer's solution are shown in Fig. 3.

The activation energies (kJ mol^{-1}) that were obtained for the alloys exposed to various solutions from both the potentiodynamic polarization and polarization resistance analysis showed reasonably close correlations (Fig. 4). The corresponding thermodynamic parameters are summarized in Table 4.

The results showed that the corrosion activation energies for the various HCl acid concentrations were similar in magnitude when compared to the activation energies of the Ringer's and 3.5 % NaCl solutions, even though the corrosion rates of the alloy at 20 °C in the respective solutions were considerably different (Table 4). This implied that the influence of temperature on the respective corrosion process as expressed through the Arrhenius equation was similar, thereby resulting in similar thermodynamic parameters, although in terms of the rate of corrosion, it was considerably different. Notably, the activation energy of the metal alloy in Ringer's solution was slightly higher and subsequently showed a larger change in enthalpy when compared to the sample that was exposed to the 3.5 % NaCl solution. This result was observed even though the corrosion rate at 20 °C was seen to be comparatively smaller for the alloy in Ringer's solution.

The activation energy of an electrochemical process can be described as the energy that must be overcome for a single electron to exchange through the electrode-electrolyte interface. Hence, the lower activation energies are indicative of an increase in the corrosion rates with an increase in temperature and *vice versa*.

The results showed that the corrosion rates of the alloy in relatively high concentrated sulphuric acid solutions were similar in magnitude to the rate of corrosion in the various

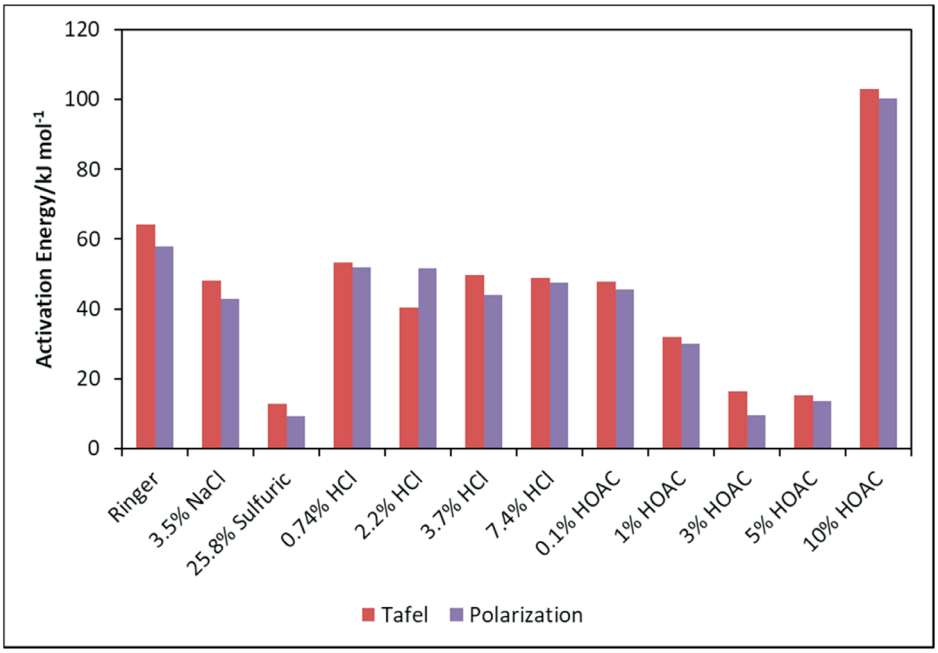

Figure 4 The activation energies determined by potentiodynamic polarization and polarization resistance measurements for all solutions studied.

Table 4 Thermodynamic parameters, namely ΔH and ΔS, for each solution determined by potentiodynamic polarization and polarization resistance measurements.

Solution	Results using potentiodynamic polarization analysis Results using polarization resistance analysis			
	E_a /kJ mol^{-1}	ΔH /kJ mol^{-1}	ΔS /J K^{-1} mol^{-1}	CR at 20 °C /10^{-5} mm yr^{-1}
Ringer	64.16	61.60	–114.33	7.52
	57.79	55.23	–130.99	12.9
3.5 % NaCl	48.11	45.56	–147.90	81.2
	43.01	45.62	–163.08	105.0
25.8 % H_2SO_4	12.74	10.18	–227.09	12500
	9.35	6.80	–235.59	18300
0.74 % HCl	53.28	50.75	–86.74	16400
	51.89	49.35	–85.11	34900
2.2 % HCl	40.44	37.89	–128.63	18700
	51.62	49.06	–92.22	17100
3.7 % HCl	49.75	47.22	–99.17	15000
	43.97	41.44	–117.34	18300
7.4 % HCl	48.80	46.27	–100.95	18600
	47.48	44.95	–100.51	33600
0.1 % HOAC	47.90	45.34	–149.74	73.4
	45.61	43.05	–155.60	93.0
1 % HOAC	31.84	29.29	–197.87	156
	30.10	27.54	–202.46	196
3 % HOAC	16.48	13.92	–249.02	200
	9.53	6.97	–269.67	288
5 % HOAC	15.22	12.66	–255.16	158
	13.59	11.04	–259.52	185
10 % HOAC	102.88	100.32	59.06	966
	100.34	97.78	51.11	1280

hydrochloric acid solutions. The slight differences between the corrosion rates at 20 °C determined by the potentiodynamic polarization and polarization resistance methods are due to the differences in their respective analytical approach.

The activation energy determination of the alloy in acetic acid solutions showed a gradual decrease over the first three lower concentrations (1 % to 5 %), with comparatively similar corrosion rates at 20 °C (Table 4). However, in a solution of 10 % acetic acid, a very large increase in the activation energy was observed with a significantly larger increase in the corrosion rate at 20 °C. This could be due to a significant increase in the passivation layer that formed on the surface of the alloy in this particular acetic acid solution. However, the study showed that the alloy exposed to the 10 % acetic acid solution had a significantly larger activation energy.

In this study, all solutions were shown to have positive values for ΔH which implied that all corrosion processes were endothermic. The ΔH component is the main constituent of the activation energy and the biggest driving force for the corrosion reaction to move forward spontaneously. However, for the alloy in the 10 % acetic acid solution, the ΔH was significantly larger than for the other solutions. The change in entropy (Δ) for all solutions, except the 10 % acetic acid, was negative, implying that the change in the Gibbs energy for the forward corrosion reaction would increase with increasing temperature. However, for the metal alloy in the 10 % acetic acid solution, the change in entropy was shown to be positive. This implied that there was a net increase in the entropy of the system, which in part includes the increase in the formation of the passivation film and that the net corrosion rate would subsequently start to decrease due to the protective layer that formed. This protective layer would form faster with an increase in temperature.

The results showed that there were no significant increases in the corrosion rates of the alloy when exposed to various concentrations of HCl of up to 7.4 %. This was also reflected in the respective activation energies observed over the acid's concentration range. The results were similar in magnitude to the reported corrosion rates of the alloy when exposed to orthophosphoric acid.[4] By obtaining the respective corrosion activation energies, it is then possible to determine the corrosion rates at higher temperatures and determine if the alloy is suitable for certain high-temperature engineering applications.

The microstructural analysis of the Inconel 600™ alloy is shown in Figs. 5 and 6.

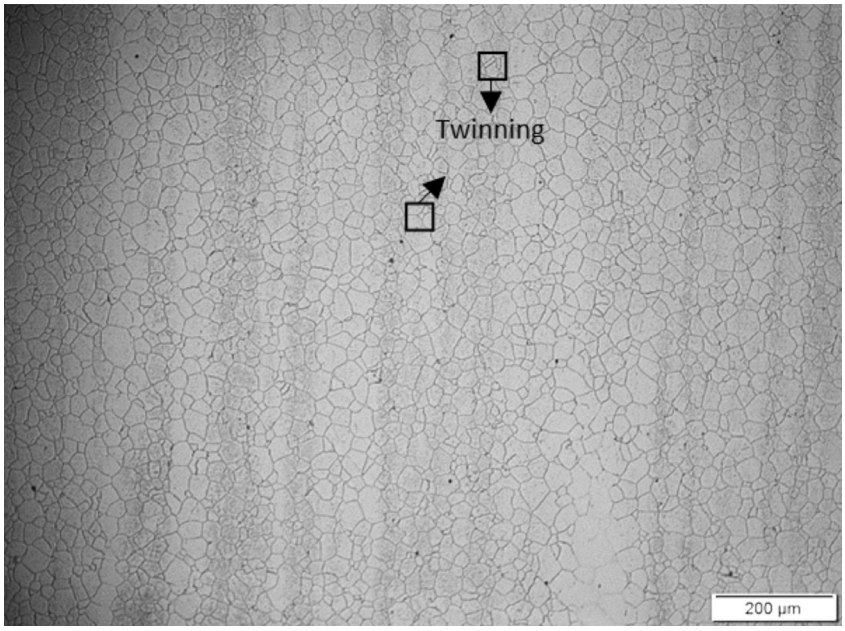

Figure 5 Optical microscope image at ×200 magnification of etched Inconel 600™ showing austenitic grain morphology with some regions displaying typical twinning.

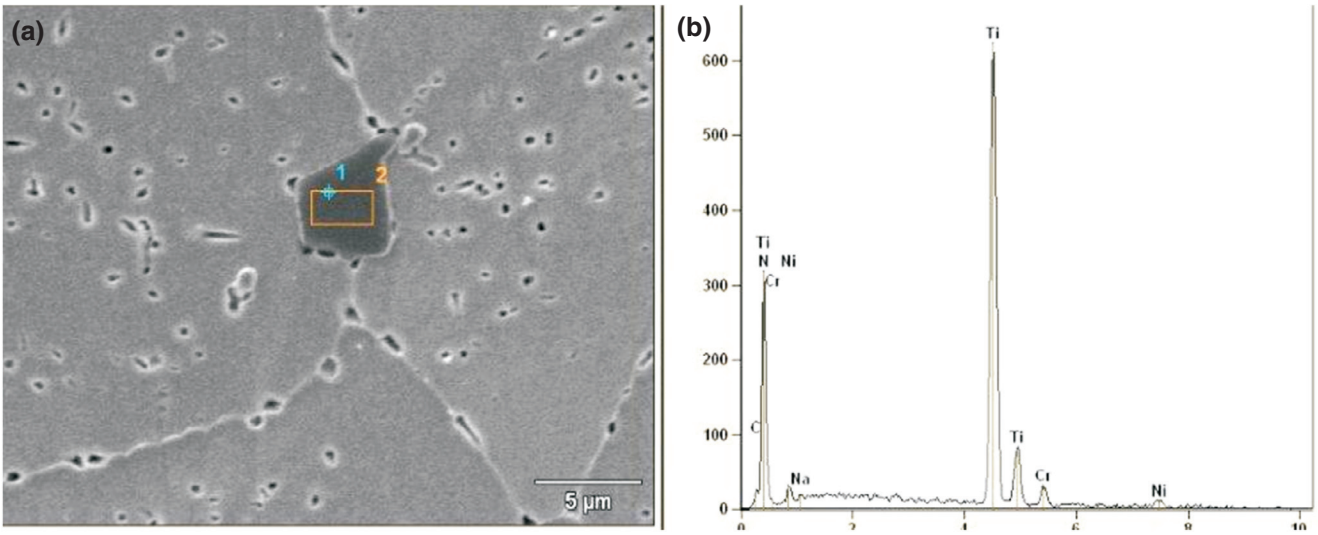

Figure 6 (**a**) ×4000 magnification of a SEM micrograph showing a TiN inclusion in the Inconel 600™ alloy. (**b**) Elemental EDS scan of the inclusion area 2 as shown in the micrograph.

The micrographs show a fine austenitic grain morphology with an average grain area of 157.06 μm^2 and an average grain diameter of 50.00 μm from the transverse micrograph. The longitudinal micrograph also showed a fine austenitic grain morphology with an average grain area of 142.86 μm^2 and an average grain diameter of 45.48 μm.

The SEM micrographs of the alloy show that there were localized inclusions or intergranular precipitates. The EDS analysis showed a high element weight percentage of Ti and N which can be in the form of TiN, which has been reported elsewhere.[12] Bertali *et al*.[13] also found that TiN had a low unison of deformation within the matrix material and can easily 'flake off' to cause a nucleation site which will then have a high stress concentration and possibly lead to stress cracking corrosion. The analyzed area showed an inclusion of about 29.7 μm^2. This was also confirmed by the studies done by Abdallah *et al*.[6–8] that showed the extent of pitting corrosion of the Inconel 600™ alloy when exposed to various acids and bases and that the grain boundary precipitates would correspond to $(Cr - Fe)_{23}C_6$ and TiN.

4. Conclusions

Potentiodynamic polarization plots and polarization resistance techniques provided a good correlation between the corrosion rates and thermodynamic activation energies obtained for the Inconel 600™ alloy in various solutions. Inconel 600™ alloy showed a relatively higher corrosion resistance when exposed to Ringer's solution thereby making it suitable for possible prosthetic applications. The alloy showed relatively similar low corrosion resistance in 25.8 % sulfuric acid and in various HCl solutions irrespective of the concentration. The study showed a relatively high corrosion resistance in weak acetic acid solutions with an unusually high activation energy for the sample in 10 % acetic acid. This was ascribed to the formation of a passivation film on the surface of the sample. The Arrhenius equation and transition state equation allowed for the calculation of thermodynamic parameters. The activation energy and transition state parameters gave an indication of the thermodynamic dependence of the corrosion process on the respective temperature changes. Even though the activation energies, changes in enthalpy and entropy were similar, their respective corrosion rates were significantly different. In general, this implied that the larger activation energies resulted in a greater corrosion resistance but also a larger dependence on temperature. Microstructure analysis classified Inconel 600™ as a fine austenite grain structure. The grain boundary precipitate and inclusion, present in the Inconel 600™, were found to be $(Cr - Fe)_{23}C_6$ and TiN, respectively, by EDS analysis.

Acknowledgements

The authors thank eNtsa (NMU) for providing the alloy samples for the study. The authors also thank the South African National Research Foundation (NRF) for financial assistance to the project.

§ORCID iD

E.E. Ferg: orcid.org/0000-0001-7231-5050

References

1 High-Performance Alloys for Resistance to Aqueous Corrosion, Special Metals Corporation, Huntington, 2000, SMC-026. http://www.specialmetals.com/assets/smc/documents/pcc-8064-sm-alloy-handbook-v04.pdf (accessed 22 October 2017).
2 Inconel® Alloy 600, UNS number N06600, *Megamex*, *speciality metals on demand*. http://www.megamex.com/inconel_600.html (accessed 26 October 2017)
3 F. Cattant, D. Crusset and D. Feron, Corrosion issues in nuclear industry today, *Mat. Today*, 2008, **11**(10), 32–37.
4 M. Vishnudevan G. Venkatachari S. Muralidharan and N.S. Rengaswamy, Corrosion behaviour of Inconel 600 and 601 in orthophosphoric acid solutions, *Anti-Cor. Meth. Mat*., 1998, **45**(4), 248–251.
5 I.B. Singh and G. Venkatachari, Anodic behaviour of Inconel 600 and 601 in sulphuric acid solutions, *Bull. Electrochem*., 1996, **12**, 83–85.
6 M. Abdallah, B.A. Al Jahdaly, M.M. Salem, A. Fawzy, E.M. Mabrouk and M. Abdallah, Electrochemical behavior of nickel alloys and stainless steel in HNO_3 using cyclic voltammetry technique, *J. Mater. Environ. Sci*., 2017, **8**(4), 1320–1327.
7 M. Abdallah, M.M. Salem, I.A. Zaafarany, A. Fawzy and A.A. Abdel Fattah, Corrosion performance of stainless steel and nickel alloys in aqueous sodium hydroxide as revealed from cyclic voltammetry and potentiodynamic anodic polarization, *Orient. J. Chem*., 2017 **33**(5), 2875–2883.
8 M. Abdallah, B.A. Al Jahdaly, M.M. Salem, A. Fawzy and A.A. Abdel Fattah, Pitting corrosion of nickel alloys and stainless steel in chloride solutions and its inhibition using some inorganic compounds, *J. Mater. Environ. Sci*., 2017, **8**(7), 2599–2607.
9 A. Balamurugan, S. Rajeswari, G. Balossier, A.H.S. Rebelo and J.M.F. Ferreira, Corrosion aspects of metallic implants – An overview. *Mater. Corros*., 2008, **59(11)**, 855–869.
10 Gamry, Getting started with electrochemical corrosion measurement, Gamry 2015, USA.

http://www.gamry.com/application-notes/corrosion-coatings/basics-of-electrochemical-corrosion-measurements/ (accessed 22 October 2017)

11 Y. Xu, Y. Xiao, D. Yi, H. Liu, L. Wu and J. Wen, Corrosion behavior of Ti–Nb–Ta–Zr–Fe alloy for biomedical applications in Ringer's solution, *Trans. Nonferrous Met. Soc. China*, 2015, **25**(8), 2556–2563.

12 ASTM E112-13, Standard testing methods for determining average grain size, ASTM International, 2012, USA.

13 H.X. Hu, Y.G. Zheng and C.P. Qin, Comparison of Inconel 625 and Inconel 600 in resistance to cavitation erosion, *Nuclear Eng. Design*, 2010, **240**, 2721–2730.

14 G. Bertali, F. Scenini and M.G. Burke, Advanced microstructural characterization of the intergranular oxidation of Alloy 600, *Corr. Sci.*, 2015, **100**, 474–483.